Computer-Assisted Radiology and Surgery

Original Investigations

Automated Lung Segmentation for Thoracic CT:

Impact on Computer-Aided Diagnosis[1]

Samuel G. Armato III, PhD , William F. Sensakovic, BA, BS

Rationale and Objectives. Automated lung segmentation in thoracic computed tomography scans is essential for the development of computer-aided diagnostic (CAD) methods. A core segmentation method may be developed for general application; however, modifications may be required for specific clinical tasks.

Materials and Methods. An automated lung segmentation method has been applied (1) as preprocessing for automated lung nodule detection and (2) as the foundation for computer-assisted measurements of pleural mesothelioma tumor thickness. The core method uses gray-level thresholding to segment the lungs within each computed tomography section. The segmentation is revised through separation of right and left lungs along the anterior junction line, elimination of the trachea and main bronchi from the lung segmentation regions, and suppression of the diaphragm. Segmentation modifications required for nodule detection include a rolling ball algorithm to include juxtapleural nodules and morphologic erosion to eliminate partial volume pixels at the boundary of the segmentation regions.

Results. For automated lung nodule detection, 4 of 82 actual nodules (4.9%) were excluded from the lung segmentation regions when the core segmentation method was modified compared with 14 nodules (17.1%) excluded without modifications. The computer-assisted quantification of mesothelioma method achieved a correlation coefficient of 0.990 with 134 manual measurements when the core segmentation method was used alone; correlation was reduced to 0.977 when the segmentation modifications, as adapted for the lung nodule detection task, were applied to the mesothelioma measurement task.

Conclusion. Different CAD applications impose different requirements on the automated lung segmentation process. The specific approach to lung segmentation must be adapted to the particular CAD task.

Keywords. Computed tomography (CT); computer-aided diagnosis (CAD); image segmentation; image processing; Chest radiology

Helical computed tomography (CT) of the thorax is widely used to evaluate numerous lung diseases, including lung nodules, emphysema, and pulmonary embolism (1). The availability of multidetector-row CT scanners has further expanded the role of CT in the diagnostic assessment of patients. These scans, however, yield a large amount of image data. The expanding volume of thoracic CT studies and the concomitant increase of image data these studies generate have prompted many investigators to develop computer-aided diagnostic (CAD) methods to assist radiologists in the evaluation of CT images (2–12). To provide useful and reliable information, most such CAD methods require identification of the lung boundaries within the images, a preprocessing step known as "lung segmentation" (4,10,12–27).

The requirement for lung segmentation is twofold. First, the pathologies that continue to motivate development of CAD schemes for thoracic CT are predominantly located within, or affect, the lungs. Consequently, these schemes are designed to accommodate the anticipated

Acad Radiol 2004; 11:1011–1021

[1] From the Department of Radiology, The University of Chicago, 5841 South Maryland Avenue, Chicago, IL 60637 (S.G.A., W.F.S.). Received February 6, 2004; accepted June 8, 2004. Presented in part at the 1999 annual meeting of the RSNA, the 1999 and 2000 annual meetings of the AAPM, and the 2003 CARS meeting. Supported in part by USPHS Grant CA83908, a grant from the Mesothelioma Applied Research Foundation, a grant from the American Lung Association of Metropolitan Chicago, and funding from The University of Chicago Cancer Research Center. **Address correspondence** to S.G.A. s-armato@uchicago.edu

doi:10.1016/j.xacra.2004.06.005

appearance of the lung regions in CT images. Moreover, spatially limiting further processing to the lungs greatly reduces computation time, because the lungs occupy a fraction of the total volume data acquired during a CT scan. Second, lung segmentation must be accurate because abnormalities such as lung nodules may exist at the extreme periphery of the lungs. If the entire lung is not segmented, such abnormalities will be lost to subsequent analyses. Moreover, quantitative assessment of lung volume for the evaluation of emphysema, for example, will be compromised by erroneous lung segmentation.

Aside from its application as a preprocessing step for CAD methods, automated lung segmentation may be useful for image data visualization. The three-dimensional display of CT image data is an area of rapid development with a number of well-documented clinical applications (28). Initial lung segmentation would be required in a situation in which, for example, a volume-rendered version of the lung parenchyma is desired as a visual aid for the radiologist's diagnostic task.

A core lung segmentation method may be used for general application; however, specific tasks may require modifications to the details of the method (29). Specifically, we have developed a fully automated technique for the segmentation of the lung regions in thoracic CT scans for use (1) as a preprocessing step for automated lung nodule detection and (2) as the basis for a computer-assisted technique to measure the extent of pleural mesothelioma. Although the essential elements of the lung segmentation methods used remain constant, important modifications are made to accommodate these two quite different clinical tasks.

MATERIALS AND METHODS

Core Segmentation Method

The automated lung segmentation method is depicted in Fig 1. Aspects of this method have been reported previously (2,10,30,31). With the exception of trachea and main bronchi elimination, which makes use of the contiguity of the airways between adjacent sections, each step is performed on a section-by-section basis. The overall method includes core techniques and also allows for the implementation of additional task-specific modifications to the lung segmentation regions.

As visualized on a CT section image, the lung regions are represented by dark (ie, low attenuation or low CT number) regions completely surrounded by a bright (ie, high attenuation or high CT number) region, which, in turn, is completely surrounded by a dark region (the air outside the patient). Lung segmentation proceeds by first segmenting the thorax from the background image data (2,30). A cumulative gray-level profile is constructed from pixels along a diagonal of the CT section image, and the shape of this profile is used to identify a gray-

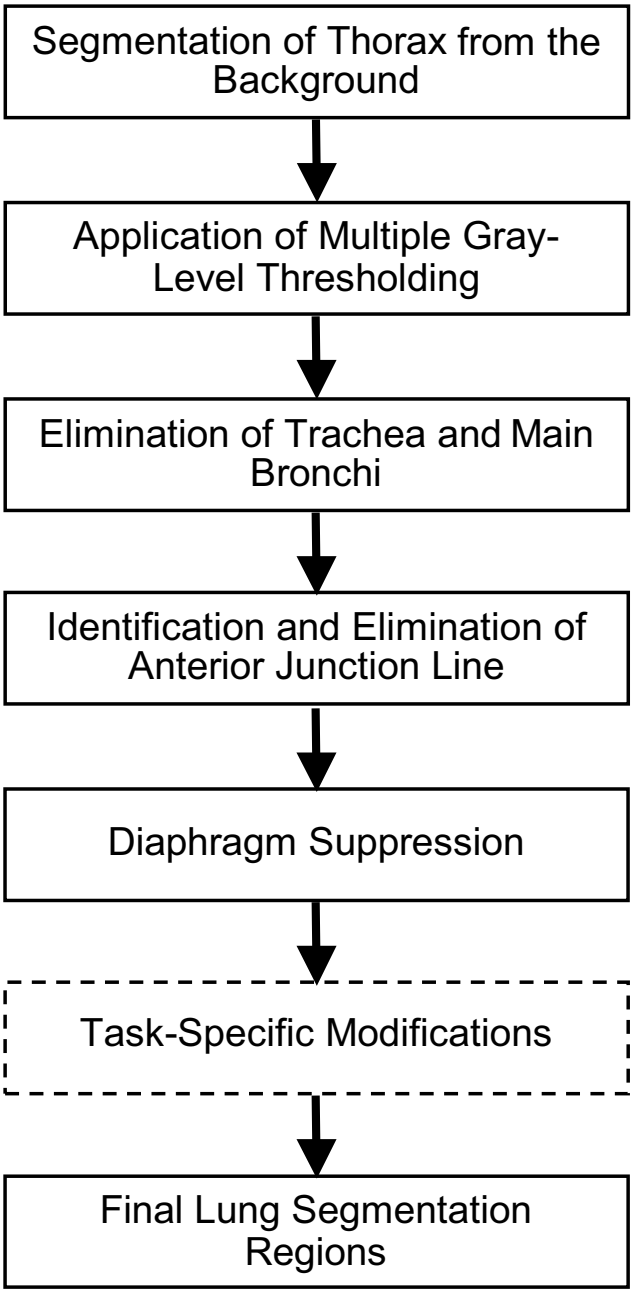

Figure 1. Automated lung segmentation includes a core technique and allows for the implementation of additional task-specific modifications.

Figure 2. The binary image that results from thresholding the segmented thorax region with the selected gray-level threshold. The resulting initial lung segmentation contours are also shown.

level threshold. A binary image is created by thresholding the section image such that a pixel is turned "on" in the binary image if the value of the corresponding pixel in the section image has a value greater than the gray-level threshold; all other pixels remain "off" in the binary image. An eight-connected border tracking algorithm (32) is used to identify the outer margin of the largest "on" region in the binary image, and the set of pixels in the original image that lie within this contour is considered the segmented thorax region.

A gray-level histogram is constructed from pixels in the segmented thorax region (2,30). The distribution of pixels in this typically bimodal histogram is used to identify a gray-level threshold value within the broad minimum in the histogram (2). This gray-level threshold is applied to the segmented thorax region to create a binary image such that a pixel is turned "on" in the binary image if the value of the corresponding pixel in the thorax segmentation region has a value less than the gray-level threshold; all other pixels remain "off" in the binary image. The eight-connected border tracking algorithm is used to identify the outer margins of the "on" regions in the binary image, and the sets of all image pixels that lie within these contours represent the segmented lung regions (Fig 2). Morphologic constraints are imposed to ensure that radiolucent nonpulmonary structures, such as bowel gas, are not erroneously identified as lung regions; for example, highly circular low-attenuation regions that may be captured by gray-level thresholding are rejected as bowel gas if they are positioned anteriorly within inferior CT sections.

The presence of a single, large lung segmentation region in any section indicates that gray-level thresholding has fused the two lung regions at the anterior junction (10,19,25,26). Distinction between left and right lungs is often required for more detailed image analysis. Consequently, the single lung region is separated into two regions by eliminating pixels along the anterior junction line. The most anterior point along the cardiac aspect of the lung region is identified. The mean pixel values along rays extending through the lung region from this point to the anterior aspect of the lung region are determined. The ray that yields the greatest mean pixel value within ± 50 degrees of vertical is identified as the initial anterior junction line. Because the anterior junction line typically demonstrates a mild curvature, a search of 10 pixels on either side of the initial anterior junction line is performed in each image row intercepted by the initial anterior junction line to locate the local maximum. This set of local maximum pixels represents the anterior junction line, which is turned "off" in the lung region to create two distinct regions from what had been erroneously identified by initial gray-level thresholding as a single segmented lung region (Fig 3).

Gray-level thresholding tends to include the trachea and main bronchi within the segmented lung regions (10). To ensure that these structures are not subsequently included in the segmented lung regions, the trachea and main bronchi are eliminated from the segmented thorax regions in all sections in which they appear. A seed point for trachea segmentation is automatically identified in the superiormost CT section. This seed point is the pixel with the lowest gray level in a region about the center-of-mass of the thorax and is assumed to exist within the trachea. A region-growing technique (32) is used to expand the identified trachea region about the seed point; as the gray-level threshold is incremented by 5 during region growing, more pixels surrounding the seed point within the trachea are identified. A stopping criterion is established to halt the region-growing process when the trachea has been adequately segmented. This stopping criterion is satisfied when the area of the trachea at iteration i is less than 5 pixels greater than the corresponding area at iteration i-1. Seed points are identified in subsequent CT sections based on the center-of-mass location of the seg-

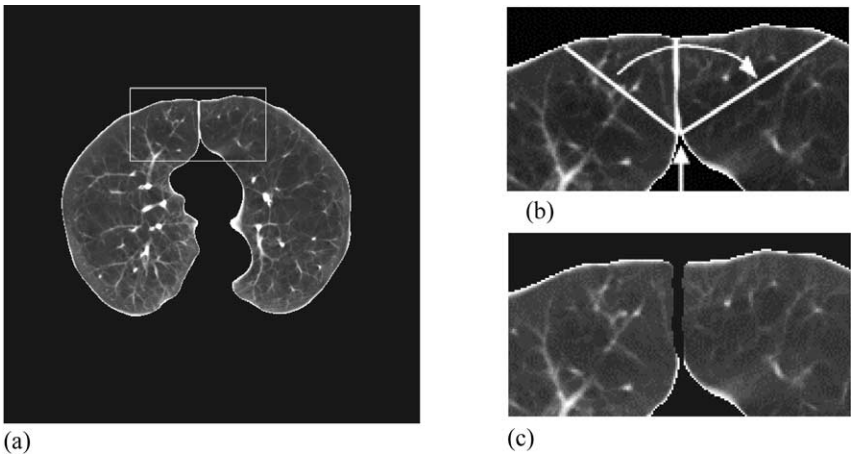

Figure 3. **(a)** A single, large lung segmentation region that spans both halves of the image indicates the presence of an anterior junction line. **(b)** After the most anterior point along the cardiac aspect of the lung segmentation region is identified (straight arrow), a series of rays is used to identify the anterior junction line, which is then turned off **(c)** to force separation into two distinct lung segmentation regions.

mented trachea region in the previous section. A sufficiently large difference between the center-of-mass location of the segmented trachea region in the previous image and the seed point location in the present image signifies that the trachea has bifurcated into the right and left main bronchi. Consequently, two seed points in each subsequent image are sought for region growing. Bronchial segmentation is not performed in images inferior to the image in which region-growing first expands the bronchi into the lung parenchyma. With the trachea and main bronchi segmented in this manner, pixels identified as belonging to the trachea or main bronchi are turned "off" so that they will not contribute to the lung segmentation regions. Figure 4 shows the effect of trachea and main bronchi elimination on the segmented lung regions.

The binary images that result from gray-level thresholding tend to contain holes of "off" pixels that are completely surrounded by "on" pixels. These holes result from denser (ie, brighter) structures contained within the lung regions that have gray levels greater than the gray-level threshold for initial lung segmentation; consequently, the corresponding pixels in the binary image remain "off." In most instances, these structures represent vessels within the lungs. Because the contouring scheme considers a segmented lung region as all pixels within the outermost boundary of an "on" region in the binary image, these dense vessels are correctly included within the segmented lung regions. The diaphragm, however, often

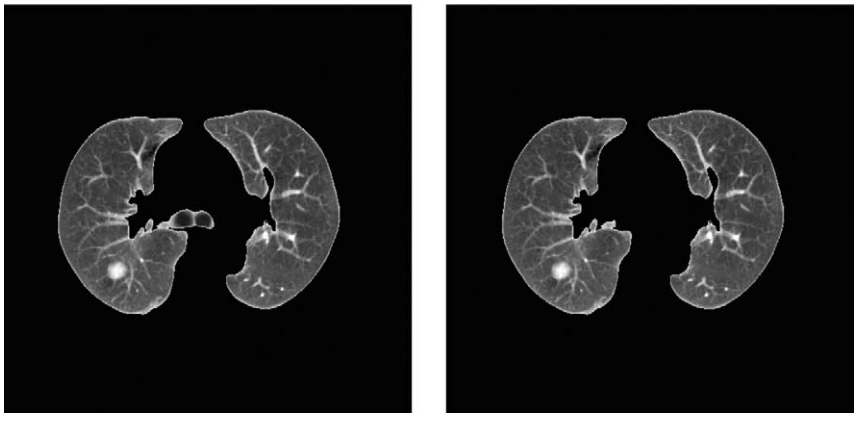

Figure 4. Lung segmentation before (left) and after (right) trachea and main bronchi elimination.

Figure 5. The diaphragm may be identified based on geometric properties of "holes" in the binary image created from gray-level thresholding. The characteristic large, circular appearance of a hole caused by the diaphragm (arrow) indicates that pixels within this area should not be included within the segmented lung region.

results in a similar hole in the binary image (Fig 5). To prevent including pixels that belong to the diaphragm, each hole in a binary image is identified. Holes that exceed the equivalent area of a 25-mm diameter circle (ie, too large to be considered a lung nodule) in a section located in the inferior one-third of the thoracic CT scan are attributed to the diaphragm, and the corresponding pixels are excluded from the segmented lung regions.

Segmentation Modifications: Nodule Detection

The core lung segmentation method is applied as a preprocessing step for the task of automated lung nodule detection in CT. The segmented lung regions based on gray-level thresholding, however, tend to exclude dense structures along the edges of the lung regions such as juxtapleural nodules and hilar vessels (Fig 6a). A rolling ball algorithm is applied to properly include these structures (30,31,33). The segmented lung regions are modified by a morphologic technique that effectively "rolls" a series of balls along the exterior aspect of the lung segmentation contours to incorporate pixels that may have been erroneously excluded after initial gray-level thresholding. A circular region (the ball) is constructed and is

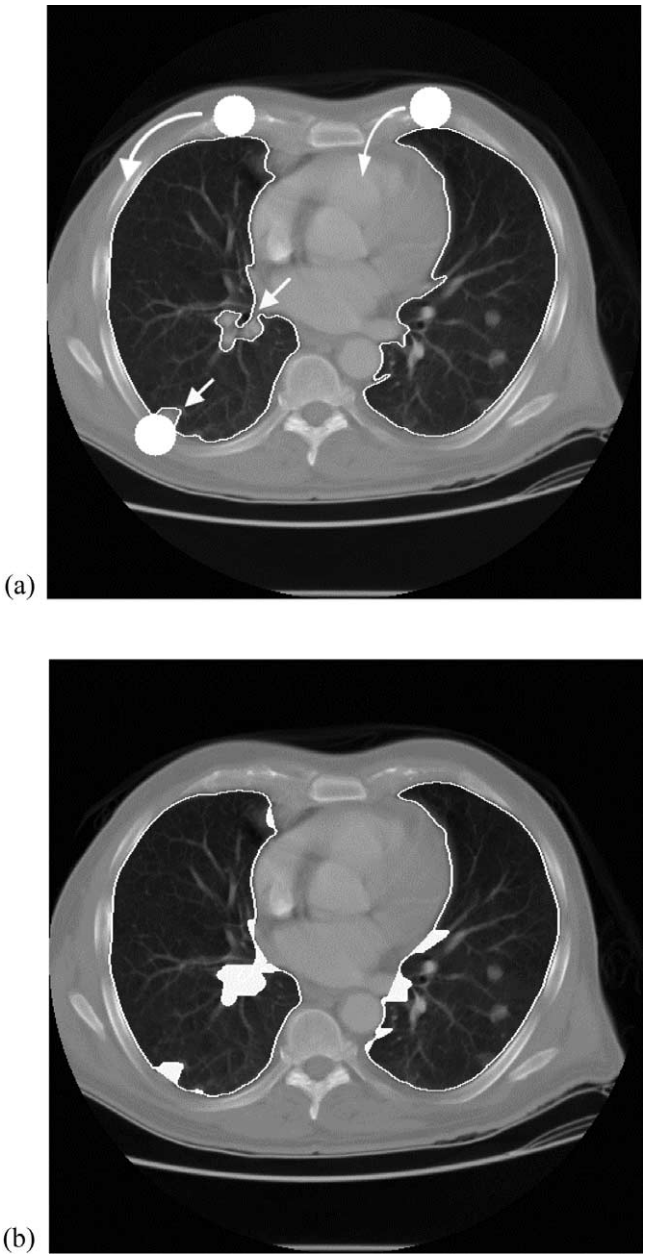

Figure 6. **(a)** Initial lung segmentation contours shown superimposed on an original section image. Gray-level thresholding tends to exclude dense structures such as juxtapleural nodules and hilar vessels (straight arrows) from the segmented lung regions. To compensate for this omission, initial placement of the two-dimensional rolling ball filter is shown along the anterior aspect of both lung segmentation contours. The filter is effectively "rolled" along the external aspect of the lung contours in the direction of the curved arrows to identify indentations, such as the one in the posterior aspect of the right lung contour. **(b)** White pixels have been included in the final lung segmentation contours after application of the rolling ball algorithm.

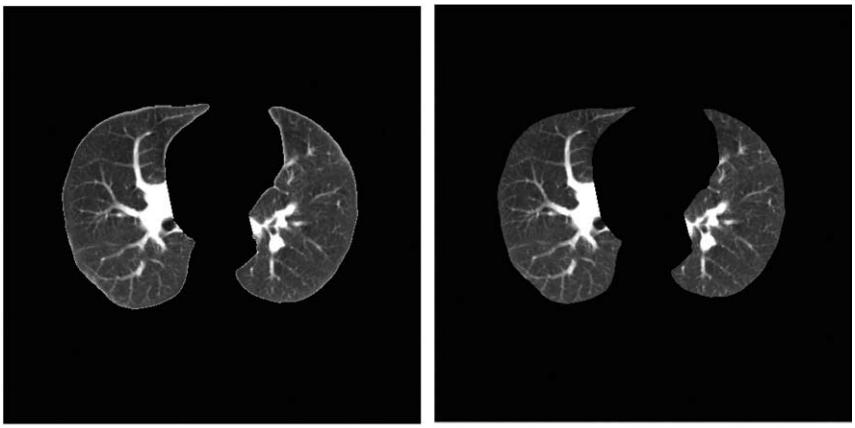

(a) (b)

Figure 7. Lung segmentation regions **(a)** before and **(b)** after morphologic erosion operator to eliminate brighter partial volume pixels along periphery of the segmentation regions.

rolled along the lung segmentation contours by successively identifying that pixel along the ball's circumference with a tangential slope that matches the tangential slope of the lung segmentation contour at the current contour pixel. The ball is positioned so that the selected ball circumference pixel is aligned with the current contour pixel. If a contour indentation of the proper scale is encountered, the ball will overlap the contour at some contour pixel other than the pixel of contact used to place the ball (Fig 6a), and this second pixel of overlap and the pixel of contact define endpoints of the contour indentation. Next, linear interpolation is used to identify new contour pixels that connect these endpoints, thus eliminating the indentation. The newly encompassed image pixels are added to the segmented lung regions (Fig 6b). An iterative, multiscale approach is used in which balls of different radii are applied in succession to rectify indentations of different dimensions. One potential pitfall of the rolling ball algorithm is that it may force inclusion of the diaphragm, even when the diaphragm has been properly excluded by gray-level thresholding. Geometric features of indentations identified by the rolling ball algorithm are computed. Based on the values of these features, the rolling ball algorithm is prevented from bridging indentations caused by the diaphragm.

Another aspect of the automated lung nodule detection method that would be adversely affected by the core lung segmentation method is the multiple gray-level thresholding technique used to identify initial lung nodule candidates. This "region-melting" method applies successively larger gray-level thresholds to the segmented lung volume derived from the set of lung segmentation regions from all sections of a scan and identifies surviving three-dimensional structures as lung nodule candidates when the volume of the structure is reduced below some upper limit (10). The core lung segmentation method, however, generates lung segmentation regions in each section that include a portion of the brighter partial volume pixels that exist near the interface of the lung and chest or mediastinum (Fig 7a). During the multiple gray-level thresholding process, these boundary pixels would be connected across CT sections to form a three-dimensional outer shell that would encapsulate the lungs and confound the identification of valid lung nodule candidates, especially near the lung periphery; moreover, many anatomic structures within the lungs would be connected to this outer shell, thus adversely affecting the morphology of the structures identified as lung nodule candidates. Accordingly, a morphologic erosion operator is applied to the initial lung segmentation regions in each section to eliminate the brighter partial volume pixels (Fig 7b).

Segmentation Modifications: Mesothelioma Measurement

The core lung segmentation method is applied as a preprocessing step for the task of acquiring semiautomated mesothelioma tumor thickness measurements in CT. For this radiologic task, a user inputs a point along the outer margin of the mesothelioma tumor at a desired measurement site (Fig 8a); computerized methods we have developed then obtain the corresponding measurement as the distance between the user-selected point

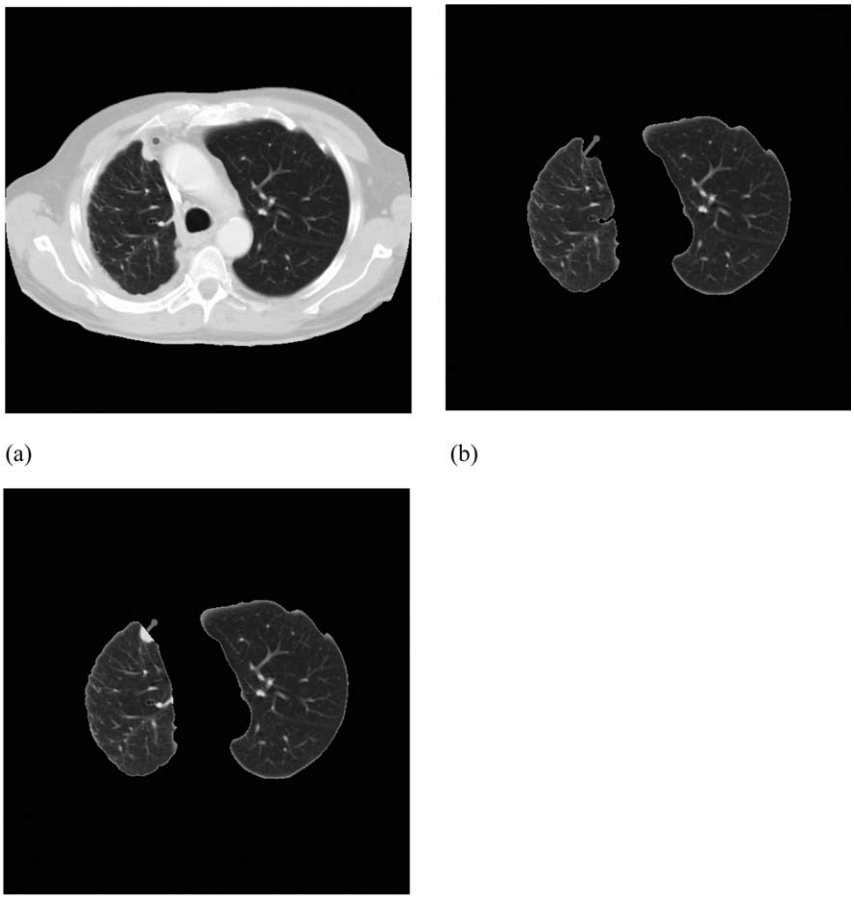

Figure 8. **(a)** Original computed tomography section demonstrating mesothelioma in the right hemithorax. A user-selected point along the outer tumor margin is shown at a desired measurement site (gray dot in white hemithorax). **(b)** The lung segmentation region generated by the core segmentation method allows a semiautomated thickness measurement that correctly spans the tumor. **(c)** With the rolling ball algorithm implemented, the boundary of the resulting lung segmentation region does not provide an appropriate surrogate for the inner tumor margin, and an underestimate of tumor thickness results.

along the outer tumor margin and a computer-determined point along the inner tumor margin, as represented by the boundary of the lung segmentation region.

Automated lung segmentation for the mesothelioma tumor thickness measurement task, however, requires neither the rolling ball algorithm nor the morphologic erosion that are used to modify the lung segmentation regions for the automated lung nodule detection task. In fact, both modifications adversely affect the mesothelioma measurements. Consider the measurement site selected in Fig 8a. Given the user-selected point along the outer tumor margin indicated in Fig 8, the computerized measurement method correctly identifies an inner tumor margin point along the boundary of the lung segmentation region generated by the core segmentation method (Fig 8b); the distance between user- and computer-selected points yields a measurement that accurately reflects tumor thickness. The tumor at this site, however, forms an indentation in the lung segmentation region generated by the core segmentation method; this indentation is eliminated if the rolling ball algorithm is implemented (Fig 8c). The boundary of the resulting lung segmentation region does not provide an appropriate surrogate for the inner tumor margin, resulting in an underestimate of tumor thickness. For the lung nodule detection task, the rolling ball algorithm is implemented to ensure that *intraparenchymal* lesions (ie, lung nodules) are correctly included within the lung segmentation regions; however, implementation of

the rolling ball algorithm for the mesothelioma tumor thickness measurement task would tend to incorrectly include *extraparenchymal* lesions (ie, mesothelioma) within the lung segmentation regions, thus adversely affecting this task.

The morphologic erosion operator applied to the lung segmentation regions to facilitate automated nodule detection is not implemented for computerized mesothelioma tumor thickness measurements. The erosion operation reduces the overall size of the lung segmentation regions, thus increasing the distance between any user-specified point along the outer tumor margin and the corresponding computer-identified point along the inner tumor margin, as represented by the boundary of the lung segmentation region. Because the resulting tumor thickness measurements tend to overestimate the manually defined values, erosion of the lung segmentation regions is not performed for this task. In fact, to reduce further the overestimation of tumor thickness, the initial lung segmentation gray-level threshold selected for this task is larger than that selected for lung nodule detection.

Databases

Two databases of thoracic CT scans were used for this study. The first database was collected for the development and evaluation of an automated lung nodule detection method (34). The second database was collected for the development and evaluation of a semiautomated method to measure mesothelioma tumor thickness (35).

Lung Nodule Database

Scans from 38 diagnostic thoracic helical CT studies were collected retrospectively from different patients (22 females, 16 males; age range 31–94 years, with a mean age of 62 years). The CT studies had been performed on GE HiSpeed scanners (GE Medical Systems, Milwaukee, WI) with a standard clinical protocol of 120 kVp, 7-mm collimation, 1.4 helical pitch, and 5-mm reconstruction interval. For some studies, sections near the lung bases deviated from the nominal reconstruction interval of 5 mm. The 38 studies comprised 1953 512 $\times$ 512-pixel section images; the number of sections per study ranged from 37 to 61, with a mean of 51 sections per study. The pixel dimensions associated with the scans ranged from 0.547 to 0.938 mm. The exposure rates used for image acquisition ranged from 220 to 300 mA, with all but five of the scans having been performed at 220 mA. All CT scans had been acquired before the commencement of this study, so that only existing image data were available for this project.

The image data were electronically transferred from the CT scanners to our research computer (SGI Onyx; Silicon Graphics, Inc., Mountain View, CA). The image data, initially acquired at 12-bit grayscale resolution, were reduced to 10 bits through a simple division of gray levels by a factor of four. Section images representing anatomy superior to the lung apices or inferior to the lung bases were manually excluded from each case.

The presence of nodules in the selected cases was reported during clinical interpretation and was noted in the radiology reports. In addition, the location of individual nodules was indicated by an experienced chest radiologist who reviewed the standard database scans on softcopy by using a computer interface. Rectangular bounding regions were placed, sized, and rotated to encompass a lesion on each CT section in which the lesion appeared, and the geometric parameters of the bounding regions for each lesion were recorded in a textual "truth" file. The 38 CT studies contained 82 lung nodules identified in this manner. Focal lesions with effective diameters that exceeded 3 cm were not considered lung nodules.

Effective diameter was computed as the mean bounding region dimension (one-half of the sum of the short and long axis lengths). When the nodule was present in more than one section, the bounding region with the greatest area was used for the effective diameter calculation. The mean effective nodule diameter was 14.7 mm. The geometric center of mass of each bounding region and the location of the maximum gray-level pixel within each bounding region were used to determine whether the automated nodule detection method correctly identified a lung nodule; if either of these pixels was contained within the set of pixels that composed a computer-extracted lung nodule candidate, that candidate was considered a "true positive."

Mesothelioma Database

The mesothelioma database consisted of 22 diagnostic thoracic helical CT scans acquired from patients with biopsy-proven malignant pleural mesothelioma. These patients (6 females, 16 males; age range 38–80 years; mean 68 years) had been enrolled in a variety of chemotherapy clinical trials at The University of Chicago Hospitals, and no scan was acquired specifically for this study. Informed consent was obtained for the research use of each patient's CT scan. No selection criteria were imposed on the scans that composed the database.

The CT examinations were performed on the GE Hi-Speed Advantage or LightSpeed CT scanners at our institution. Each CT section was reconstructed as a 512 × 512-pixel image matrix. The scans were acquired at 120 kVp with a collimation of 7 mm ($n = 18$), 7.5 mm ($n = 1$), 5 mm ($n = 1$), or 10 mm ($n = 2$). The helical pitch for different scans ranged from 1.0 to 1.4. The reconstruction interval was 10 mm for scans with 10-mm collimation and 5 mm for most of the sections in all other scans. The pixel dimensions associated with the scans ranged from 0.554 to 0.808 mm. The exposure rates used for image acquisition ranged from 190 to 220 mA.

RESULTS

Nodule Detection Results

The automated lung nodule detection method achieved 71% nodule detection sensitivity with an average of 0.4 false-positive detections per section on a database of 38 CT scans (34). The effect of lung segmentation on these results may be appreciated through the observation that of the 82 actual lung nodules in this 38-case database, only 4 nodules (4.9%) were excluded from the lung segmentation regions when the core lung segmentation method was modified by the rolling ball algorithm and the morphologic erosion operator previously described as appropriate for the automated lung nodule detection task. Without these segmentation modifications, 14 nodules (17.1%) were excluded from the lung segmentation regions obtained from the core segmentation method alone. Nodules excluded from the lung segmentation regions were lost to all subsequent analyses and, in effect, directly became false negatives.

Mesothelioma Tumor Thickness Measurement Results

The method for the computer-assisted quantification of mesothelioma achieved a correlation coefficient of 0.990, with the average manual measurements of five observers based on 134 measurement sites in 22 CT scans (35) when the core lung segmentation method was used alone. The correlation coefficient was reduced to 0.977 when the segmentation modifications, as adapted for the automated lung nodule detection task, were applied to the mesothelioma measurement task. Bland-Altman plots (36) provide another way to appreciate the differences in agreement between mesothelioma tumor thickness measurements of the average of five observers and computer-assisted measurements derived from (1) the core lung segmentation method (Fig 9a) and (2) the core segmentation method modified with the rolling ball algorithm and the morphologic erosion operator (as required for the automated lung nodule detection task) (Fig 9b). In these plots, the difference between the tumor thickness measurements of the average of five observers and the computer-assisted measurements derived from the core lung segmentation method (Fig 9a) and those derived from the core method plus modifications (Fig 9b) for each of the 134 measurement sites is plotted against the mean measurement of the average of five observers and the corresponding computer-assisted measurement at each site. Agreement between the computer and the observers can be assessed by examining the measurement differences and their dependence on the measurement magnitude. The mean difference between the average of five observers and the computer-assisted measurements derived from the core lung segmentation method is 0.055 ± 1.31 and the 95% limits of agreement for the differences are $(-2.68, 2.57)$ (Fig 9a), whereas the mean difference between the average of five observers and the computer-assisted measurements derived from the core method *plus* modifications is larger at 0.16 ± 1.98 and the 95% limits of agreement for the differences are wider at $(-3.80, 4.12)$ (Fig 9b).

CONCLUSION

We have developed automated lung segmentation methods that provide an important part of our CAD research for thoracic CT scans. These methods have been successfully applied to the automated detection of lung nodules and to the computer-assisted measurement of mesothelioma. The present study demonstrates that the lung segmentation method used as preprocessing for CAD applications may affect CAD results. The core lung segmentation method yielded lung regions that excluded 17.1% of the lung nodules in a database of 38 CT scans, whereas a modified lung segmentation method excluded only 4.9% of the nodules in this database. Conversely, when applied to a 22-case database of CT scans from mesothelioma patients, the modified lung segmentation method that proved beneficial to the lung nodule detection task generated tumor thickness measurements with a correlation coefficient of 0.977 with manual measurements, whereas the core lung segmentation method alone achieved a correlation coefficient of 0.990. Consequently, investigators should consider carefully the lung segmenta-

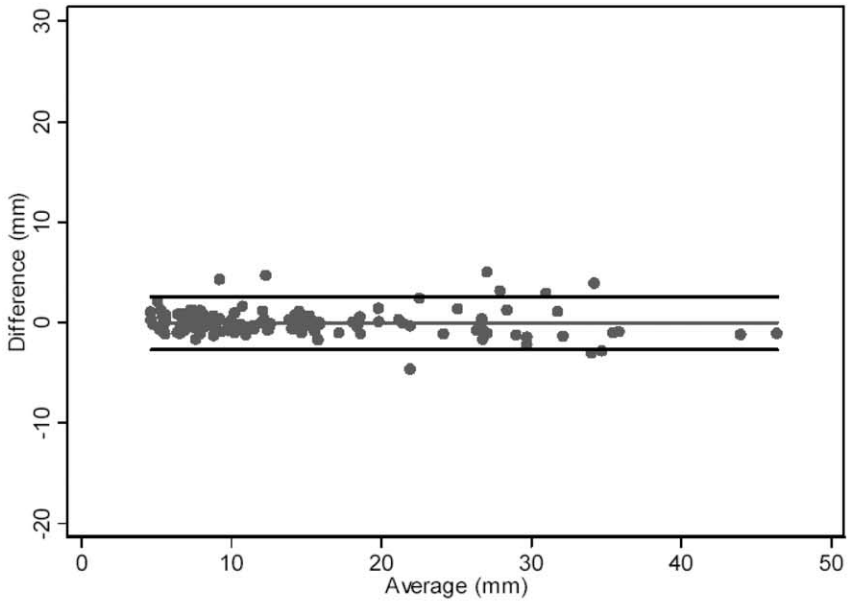

(a)

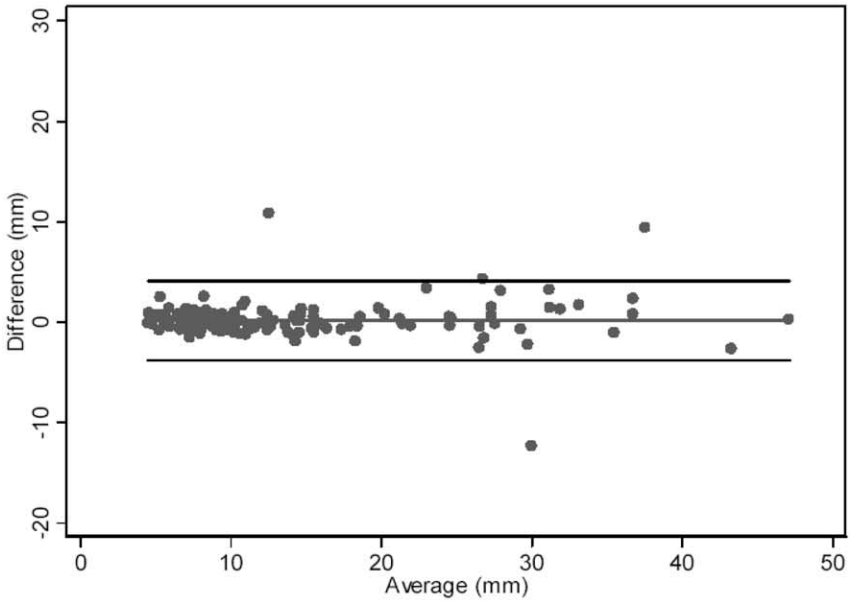

(b)

Figure 9. Bland-Altman plots obtained from the mesothelioma tumor thickness measurements of the average of five observers and **(a)** the computer-assisted measurements derived from the core lung segmentation method (reprinted with permission from (35)) and **(b)** the computer-assisted measurements derived from the core method plus modifications for each of the 134 measurement sites. Horizontal lines in the plots represent the mean difference and the 95% limits of agreement of the difference.

tion requirements imposed by the specific CAD application, and automated lung segmentation must be adapted to the specific clinical task.

ACKNOWLEDGMENT

The authors would like to thank Heber MacMahon, MD, Masha Kocherginsky, PhD, Maryellen L. Giger, PhD, Nicholas J. Vogelzang, MD, Hedy L. Kindler, MD, Carl J. Vyborny, MD, PhD, John Fennessy, MD, Feng Li, MD, PhD, Geoffrey R. Oxnard, BA, Michael B. Altman, BA, Adam Starkey, and Tamara Thompson, RN, for their assistance.

REFERENCES

1. Remy-Jardin M, Remy J. Spiral CT of the Chest. Berlin: Springer-Verlag; 1996.
2. Giger ML, Bae KT, MacMahon H. Computerized detection of pulmonary nodules in computed tomography images. Invest Radiol 29:1994; 459–465.
3. Ryan WJ, Reed JE, Swensen SJ, Sheedy PF. Jr. Automatic detection of pulmonary nodules in CT. In: Lemke HU, Vannier MW, Inamura K, Farman AG, eds. Computer assisted radiology (CARS '96). Amsterdam: Elsevier Science; 1996. p. 385–389.
4. Sakai N, Mishima M, Nishimura K, Itoh H, Kuno K. An automated method to assess the distribution of low attenuation areas on chest CT scans in chronic pulmonary emphysema patients. Chest 1994;106:1319–1325.
5. Uppaluri R, Mitsa T, Sonka M, Hoffman EA, McLennan G. Quantification of pulmonary emphysema from lung computed tomography images. Am J Respir Crit Care Med 156:1997;248–254.
6. Okumura T, Miwa T, Kako J, et al. Image processing for computer-aided diagnosis of lung cancer screening system by CT (LSCT). Proc SPIE 1998;3338:1314–1322.
7. Fiebich M, Wietholt C, Renger BC, et al. Automatic detection of pulmonary nodules in low-dose screening thoracic CT examinations. Proc SPIE 1999; 3661:1434–1439.
8. Taguchi H, Kawata Y, Niki N, et al. Lung cancer detection based on helical CT images using curved surface morphology analysis. Proc SPIE 1999;3661:1307–1314.
9. Lou S-L, Chang C-L, Lin K-P, Chen T-S. Object-based deformation technique for 3-D CT lung nodule detection. Proc SPIE 1999;3661:1544–1552.
10. Armato SG III, Giger ML, MacMahon H. Automated detection of lung nodules in CT scans: preliminary results. Med Phys 2001;28:1552–1561.
11. Masutani Y, MacMahon H, Doi K. Computerized detection of pulmonary embolism in spiral CT angiography based on volumetric image analysis. IEEE Trans Med Imaging 21:2002;1517–1523.
12. Brown MS, Goldin JG, McNitt-Gray MF, et al. Knowledge-based segmentation of thoracic computed tomography images for assessment of split lung function. Med Phys 27:2000;592–598.
13. Kanazawa K, Kawata Y, Niki N, et al. Computer-aided diagnosis for pulmonary nodules based on helical CT images. Comput Med Imaging Graph 22:1998;157–167.
14. Morgan M. Detection and quantification of pulmonary emphysema by computed tomography: a window of opportunity. Thorax 1992;47:1001–1004.
15. Uppaluri R, Hoffman EA, Sonka M,Hartley PG, Hunninghake GW, McLennan G. Computer recognition of regional lung disease patterns. Am J Respir Crit Care Med 160:1999;648–654.
16. Bankier AA, de Maertelaer V, Keyzer C, Gevenois PA. Pulmonary emphysema: Subjective visual grading versus objective quantification with macroscopic morphometry and thin-section densitometry. Radiology 1999;211:851–858.
17. Zagers R, Vrooman HA, Aarts NJ, Stolk J, Schultze Kool LJ, van Voorthuisen E, Reiber JH. Quantitative analysis of computed tomography scans of the lungs for the diagnosis of pulmonary emphysema: a validation study of a semiautomated contour detection technique. Invest Radiol 1995;30:552–562.
18. Kalender WA, Fichte H, Bautz W, Skalej M. Semiautomatic evaluation procedures for quantitative CT of the lung. J Comp Assist Tomogr 15: 1991;248–255.
19. Brown MS, McNitt-Gray MF, Mankovich NJ, et al. Method for segmenting chest CT image data using an anatomical model: preliminary results. IEEE Trans Med Imaging 16:1997;828–839.
20. Brown MS, McNitt-Gray MF, Goldin JG, et al. Automated measurement of single and total lung volume from CT. J Comp Assist Tomogr 23: 1999;632–640.
21. Preteux F, Grenier P, Vanier P. Advances in automated lungs segmentation in CT studies. Proc SPIE 1898:1993;330–341.
22. Hedlund LW, Anderson RF, Goulding PL, Beck JW, Effmann EL, Putman CE. Two methods for isolating the lung area of a CT scan for density information. Radiology 144:1982;353–357.
23. Keller JM, Edwards FM, Rundle R. Automatic outlining of regions on CT scans. J Comp Assist Tomogr 5:1981;240–245.
24. Cassell KJ, France AD, Johnson N. Automatic outlining technique for EMI scanner pictures. Med Biol Eng Computing 17:1979;693–694.
25. Leader JK, Zheng B, Rogers RM, et al. Automated lung segmentation in X-ray computed tomography: Development and evaluation of a heuristic threshold-based scheme. Acad Radiol 10:2003;1224–1236.
26. Hu S, Hoffman EA, Reinhardt JM. Automatic lung segmentation for accurate quantitation of volumetric X-ray CT images. IEEE Trans Med Imaging 20:2001;490–498.
27. Hoffman EA, Reinhardt JM, Sonka M, et al. Characterization of the interstitial lung diseases via density-based and texture-based analysis of computed tomography images of lung structure and function. Acad Radiol 10:2003;1104–1118.
28. Calhoun PS, Kuszyk BS, Heath DG, Carley JC, Fishman EK. Three-dimensional volume rendering of spiral CT data: Theory and method. RadioGraphics 1999;19:745–764.
29. Armato SG III, MacMahon H, Automated lung segmentation and computer-aided diagnosis for thoracic CT scans. In: Lemke HU, Vannier MW, Inamura K, Farman AG, Doi K, Reiber JHC, eds. Computer assisted radiology and surgery (CARS 2003). Amsterdam: Elsevier; 2003. p. 977–982.
30. Armato SG III, Giger ML, Moran CJ, Blackburn JT, Doi K, MacMahon H. Computerized detection of pulmonary nodules on CT scans. RadioGraphics 19:1999;1303–1311.
31. Armato SG III, Giger ML, Moran CJ, Blackburn JT, Doi K, MacMahon H. Automated detection of pulmonary nodules in helical computed tomography images of the thorax. Proc SPIE 1998;3338:916–919.
32. Sonka M, Hlavac V, Boyle R. Image processing, analysis, and machine vision. Pacific Grove, CA: Brooks/Cole Publishing Company; 1999.
33. Armato SG III, Giger ML, Blackburn JT, Blackburn JT, Doi K, MacMahon H. Three-dimensional approach to lung nodule detection in helical CT. Proc SPIE 3661:1999; 553–559.
34. Armato SG III, Altman MB, LaRivière PJ. Automated detection of lung nodules in CT scans: effect of image reconstruction algorithm. Med Phys 2003;30:461–472.
35. Armato SG III, Oxnard GR, MacMahon H, et al. Measurement of mesothelioma on thoracic CT scans: a comparison of manual and computer-assisted techniques. Med Phys 31:2004; 1105–1115.
36. Bland JM, Altman DG. Statistical methods for assessing agreement between two methods of clinical measurement. Lancet 1:1986;307–310.